九州大学学術情報リポジトリ
Kyushu University Institutional Repository

Photoelectron Imaging Signature for Selective Formation of Icosahedral Anionic Silver Cages Encapsulating Group 5 Elements: M@Ag_12^- (M = V, Nb, and Ta)

Suzuki, Yuta
Department of Chemistry, Faculty of Science, Kyushu University

Matsumoto, Kazuaki
Department of Chemistry, Faculty of Science, Kyushu University

Nomi, Rin
Department of Chemistry, Faculty of Science, Kyushu University

Arakawa, Masashi
Department of Chemistry, Faculty of Science, Kyushu University

他

https://hdl.handle.net/2324/7178545

出版情報：The Journal of Physical Chemistry Letters. 15 (16), pp.4327-4332, 2024-04-15. American Chemical Society
バージョン：
権利関係：© 2024 The Authors

KYUSHU UNIVERSITY

Photoelectron Imaging Signature for Selective Formation of Icosahedral Anionic Silver Cages Encapsulating Group 5 Elements: $M@Ag_{12}^{-}$ (M = V, Nb, and Ta)

Yuta Suzuki, Kazuaki Matsumoto, Rin Nomi, Masashi Arakawa, Takuya Horio, and Akira Terasaki**

Department of Chemistry, Faculty of Science, Kyushu University, 744 Motooka, Nishi-ku, Fukuoka 819-0395, Japan

Corresponding Authors

*horio@chem.kyushu-univ.jp, *terasaki@chem.kyushu-univ.jp

Abstract

An assembly of thirteen atoms can form highly symmetric architectures like those belonging to D_{3h}, O_h, D_{5h}, and I_h point groups. Here, using photoelectron imaging spectroscopy in combination with density functional theory (DFT) calculations, we present a simple yet convincing experimental signature for selective formation of icosahedral cages of anionic silver clusters encapsulating a dopant atom of group 5 elements: $M@Ag_{12}^-$ (M = V, Nb, and Ta). Their photoelectron images obtained at 4 eV closely resemble one another: only a single ring is observed, which is assignable to photodetachment signals from a five-fold degenerate superatomic 1D electronic shell in the $1S^2 1P^6 1D^{10}$ configuration of valence electrons. The perfect degeneracy represents an unambiguous fingerprint of an icosahedral symmetry, which would otherwise be lifted in all the other structural isomers. DFT calculations confirm that I_h forms are the most stable and that D_{5h}, O_h, and D_{3h} structures are not found even in metastable states.

TOC GRAPHICS

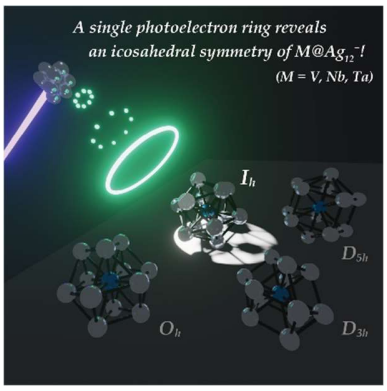

KEYWORDS

Icosahedron, Structural determination, Geometric isomer selectivity, Metal clusters, Superatoms, Group theory, Photoelectron imaging

Twelve atoms can build up highly symmetric cages like those belonging to D_{3h}, O_h, D_{5h}, and I_h point groups, suggesting that an assembly of thirteen atoms, i.e., one at the center with the other twelve in the outer layer, is expected to be a distinctive nanocluster. Especially, an icosahedron is the best known as an iconic structure in the finite size regime,[1] where a magic number of n = 13 was observed in the mass spectra of rare gas clusters, R_n (R = Ar[2] and Xe[3]), implying that R_{13} is the smallest size of so-called Mackay icosahedra with concentric shell structures.[4] The aluminum tridecamer anion, Al_{13}^-, is one of the most well-known metal aggregates with I_h symmetry that has been inspiring a considerable body of work on so-called *superatoms*.[5,6] Icosahedral forms also constitute novel platforms for synthesizing ligand-protected gold and silver superatoms,[7] leading to a variety of promising applications based on atomically-precise metal nanoclusters.

Such highly symmetric architectures are also formed by an assembly of twelve atoms, A_{12}, encapsulating a foreign atom, X, at the center of the A_{12} cage, i.e., $X@A_{12}$. The diversity of the combinations of A and X has stimulated a bunch of experimental and theoretical explorations for discovering $X@A_{12}$, which are summarized in a part of a recent comprehensive review by Zhao et al.[8] Among them, X-doped coinage metal clusters (i.e., A = Cu, Ag, and Au) have been attracting much attention.

Pyykkö and Runeberg[9] explored the most stable structure of $W@Au_{12}$ using density functional theory (DFT), where they predicted that $W@Au_{12}$ is in I_h symmetry with eighteen valence electrons ($12\times$Au $6s^1$ + W $6s^25d^4$) delocalized over the metal framework with the spin multiplicity of singlet. This suggests that the jellium model,[10] which is known to well describe valence electrons in clusters of monovalent metals (Na_n, Au_n, etc.), can also be applied to this bimetallic cluster; the valence electrons occupy atomic-like electronic shells of 1S, 1P, 1D, 2S, etc.

so that electronic-shell closure with $1S^21P^61D^{10}$ configuration is realized in W@Au_{12}. Photoelectron spectroscopy (PES) of its anion, $Au_{12}W^-$, performed by Li et al.[11] observed a sharp peak at the vertical detachment energy (VDE) as low as 2.08 eV, implying that the structural deformation upon photodetachment is minimal. Although the experiment did not directly probe the neutral species, the observation strongly suggests that the excess electron is weakly attached on a rigid icosahedral core of W@Au_{12}.

Here, we focus on $Ag_{12}M^-$ (M = V, Nb, and Ta), which are all expected to be valence iso-electronic to W@Au_{12}; $Ag_{12}M^-$ (M = V, Nb, and Ta) have commonly 18 valence electrons including the excess charge since the valence electron configurations of Ag, V, Nb and Ta atoms are $5s^1$, $4s^23d^3$, $5s^14d^4$ and $6s^25d^3$, respectively. The present study was inspired by our recent experiment on reactivities of Ag_nV^- with molecular oxygen,[12] where the size-dependent pseudo first-order reaction rate constant was revealed to exhibit a local minimum at n = 12, indicating that $Ag_{12}V^-$ is highly stable against O_2 exposure. This readily implies that the closed electronic shell structure of $1S^21P^61D^{10}$ is realized in $Ag_{12}V^-$ as well. Although information on the symmetry of the cluster's geometry was not obtained through the reactivity experiment, our DFT calculations have predicted that the doped cluster has I_h symmetry, which motivated us to apply anion PES by using our novel photoelectron imaging apparatus that enables fast acquisition of photoelectron images under space-charge free conditions.[13] As explained later, photodetachment signals from a five-fold degenerate 1D electronic shell can be an unambiguous fingerprint for I_h symmetry of V@Ag_{12}^-. This point has not been examined before. The study is extended also to $Ag_{12}Nb^-$ and $Ag_{12}Ta^-$ to explore if they are in icosahedral symmetry. After presenting our results, comparison to the anion PES studies for $Au_{12}M^-$ (M = V, Nb, and Ta) by Zhai et al.,[14] which also have 18 valence electrons, will be made by addressing possible geometric isomers in both systems.

Experimental results are presented in Figs. 1(a) – (c), which show two-dimensional (2D) projections of three-dimensional (3D) distributions for photoelectrons detached from $Ag_{12}M^-$ (M = V, Nb, and Ta), respectively, by linearly-polarized, ultraviolet (UV) femtosecond (fs) laser pulses at 310 nm (4.00 eV). From these images, we have obtained 2D slices of the original 3D photoelectron distributions, which are presented in Figs. 1(d) – (f) correspondingly. These 2D-slice images closely resemble one another, indicating that they are indeed valence iso-electronic systems. Most importantly, the 2D slice images all exhibit a *single* ring.

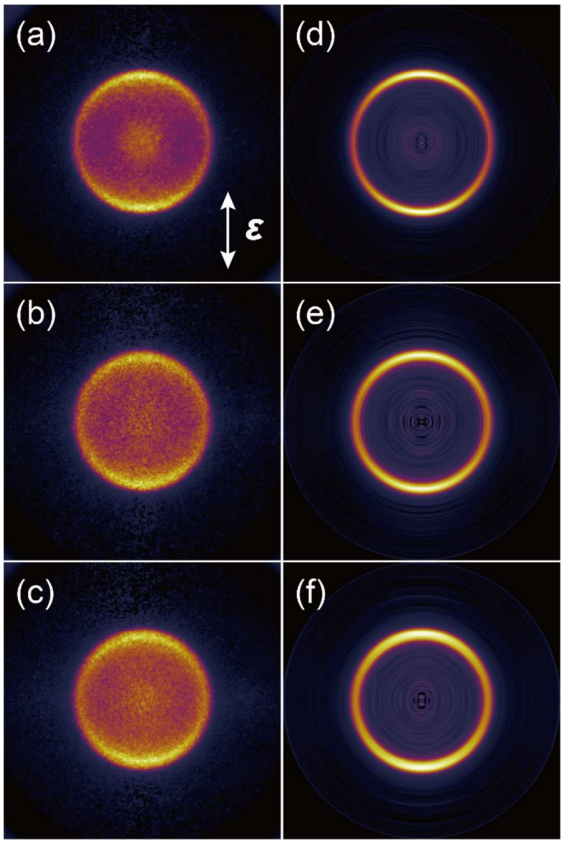

Figure 1. 2D projections (left panels) and 2D slices (right panels) of the 3D photoelectron distributions obtained for $Ag_{12}V^-$ ((a) and (d)), $Ag_{12}Nb^-$ ((b) and (e)), and $Ag_{12}Ta^-$ ((c) and (f)). The direction of the polarization vector, ε, of the 310-nm fs UV pulses is indicated by a double arrow in (a).

According to the jellium model, the valence electron configurations of $Ag_{12}M^-$ (M = V, Nb, and Ta) are predicted to be $1S^2 1P^6 1D^{10}$, where photodetachment from the outermost 1D electronic shell yields photoelectron signals with the lowest electron binding energy. Herein, we discuss how the 1D electronic shell, i.e., the highest occupied molecular orbital (HOMO), behaves under I_h, D_{5h}, O_h, and D_{3h} structures. As shown in Fig. 2, under I_h point group, the 1D electronic shell has five-fold degeneracy with h_g symmetry, whereas it splits into $e''_1 + a'_1 + e'_2$, $e_g + t_{2g}$, and $e'' + e' + a'_1$ orbitals under D_{5h}, O_h, and D_{3h} point groups, respectively. In the zeroth order approximation, where Jahn–Teller distortion and spin–orbit coupling in the neutral states are both ignored, the photodetachment signal from h_g, $e''_1 + a'_1 + e'_2$, $e_g + t_{2g}$, and $e'' + e' + a'_1$ orbitals should yield one, three, two, and three bands, respectively. Turning to the top panels of Figs. 3(a) – (c) that present experimental photodetachment spectra for $Ag_{12}M^-$ (M = V, Nb, and Ta), a *single* band is observed; it corresponds to the single ring in each image of Figs. 1(a) – (c). Thus, our results indicate the first case. This point is further discussed in spectral simulation shown later.

It should be noted that the observation of the single band for each spectrum is rather surprising, as photodetachment spectra for metal cluster anions composed of more than ten atoms are generally congested in the electron binding energy range from 0 to 4 eV; see refs.[14–16] , for example. Least-squares fitting to the observed photodetachment spectra was performed to characterize their overall spectral profiles. The dashed lines in the top panels of Figs. 3(a) – (c) are the best-fit curves using Lorentzian functions. Notably, tails in both the lower and higher energy regions of the single bands are likely due to the instrumental response of our setup, because such tails are also discernible in the photodetachment spectrum of Ag^- (see Fig. S1 in Supporting Information). In addition to these tails, minor components are observed around 4 eV in the experimental data. These are presumably due to residuals in the background subtraction, which

corresponds to weak signals in the central part of the images in Figs. 1(a) – (c) (see EXPERIMENTAL METHODS). The analysis indicates that the observed photodetachment spectra for $Ag_{12}M^-$ (M = V, Nb, and Ta) are almost symmetric to the peak energy.

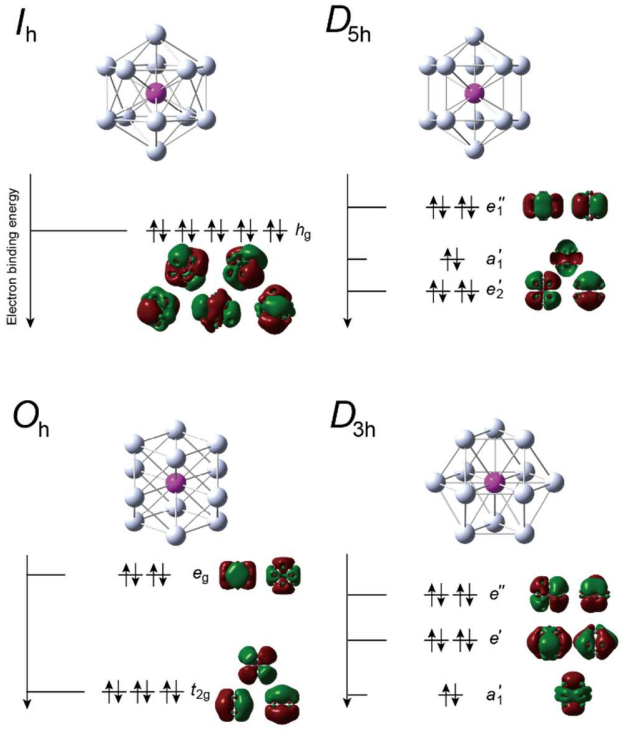

Figure 2. Possible highly-symmetric structures of $Ag_{12}M^-$ (M = V, Nb, and Ta) with their splitting schemes of the 1D electronic shells. The isosurface plots are of $Ag_{12}Ta^-$, where Kohn–Sham orbitals are shown with the isovalue of 0.01. Photodetachment signals expected for the corresponding structures are also shown schematically.

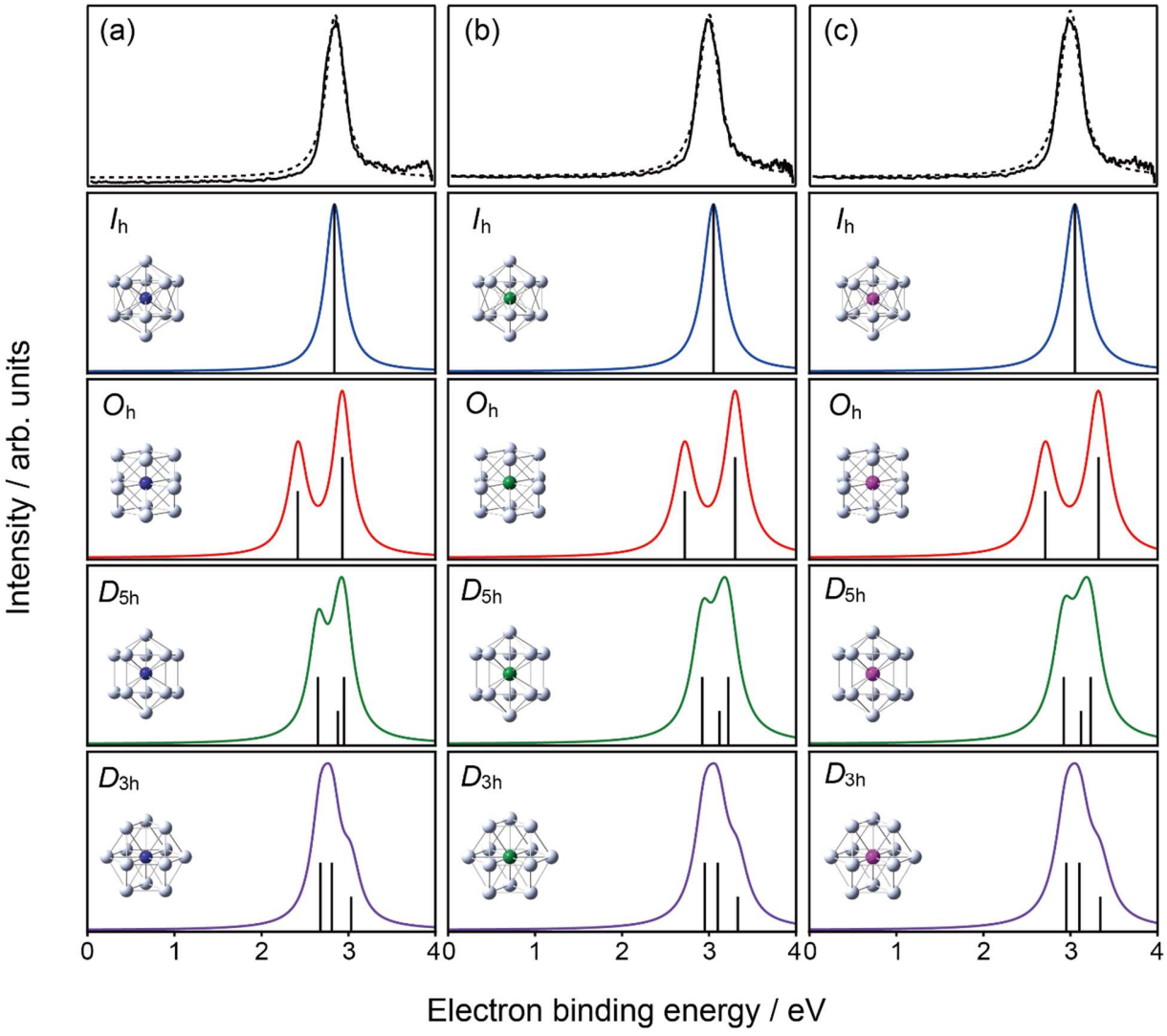

Figure 3. Photodetachment spectra (solid lines in the top panels) obtained for (a) $Ag_{12}V^-$, (b) $Ag_{12}Nb^-$, and (c) $Ag_{12}Ta^-$ with a detachment laser at 310 nm (4.00 eV). The best-fit curves using Lorentzian functions are shown with dashed lines. Simulated spectral profiles assuming I_h, D_{5h}, O_h, and D_{3h} structures, which are obtained from discrete spectra shown with vertical sticks, are presented in the lower panels (see the text).

We performed DFT calculations for exploring the most stable geometries of $Ag_{12}M^-$ (M = V, Nb, and Ta) starting from 80 initial geometries of endohedrally- or exohedrally-doped structures, the former of which included I_h, D_{5h}, O_h, and D_{3h} structures. By referring to the theoretical

investigation on $Ag_nV^{+/0}$ ($4 \leq n \leq 15$) by Medel et al.,[17] the spin multiplicity was restricted to singlet and triplet. The DFT calculations were conducted by the Gaussian 16 package[18] using possible combinations of BP86[19,20] and PBEPBE[21] functionals with SDD[22,23] and LanL2DZ[24] basis sets. We found, for all the combinations of functionals and basis sets examined, that $M@Ag_{12}^-$ (M = V, Nb, and Ta) with I_h symmetry was the most stable with the spin multiplicity of singlet and that *no* local minima were obtained for D_{5h}, O_h, and D_{3h} structures. We then evaluated their VDEs by calculating the total energy difference between $Ag_{12}M^-$ and the corresponding neutrals, $Ag_{12}M$, in their ground electronic states that have exactly the same geometries as anionic $Ag_{12}M^-$. The results obtained using BP86/SDD level are summarized in Table 1 along with the experimental values. The calculated VDEs for $M@Ag_{12}^-$ (M = V, Nb, and Ta) with I_h symmetry are in excellent agreement with the experimental ones. Although the D_{5h}, O_h, and D_{3h} structures are not in local minima, we calculated VDEs also for these structures in the same manner as mentioned above, which are presented in Table 1 as well; however, the agreement is worse. The VDEs calculated by the other combinations of functionals and basis sets are summarized in Table S1 of Supporting Information.

154 Table 1. Simulated VDEs for $Ag_{12}M^-$ (M = V, Nb, and Ta) with I_h, D_{5h}, O_h, and D_{3h} symmetries
155 at the BP86/SDD level along with the experimental VDEs and their relative total energies (in eV
156 units) shown in the parentheses.

	Vertical detachment energy (VDE) / eV				
	Expt.	Calc.			
		I_h	D_{5h}[a]	O_h[a]	D_{3h}[a]
$Ag_{12}V^-$	2.88 ± 0.02	2.84 (0)	2.65 (0.68)	2.42 (0.69)	2.68 (0.75)
$Ag_{12}Nb^-$	3.02 ± 0.02	3.05 (0)	2.92 (0.41)	2.72 (0.45)	2.95 (0.45)
$Ag_{12}Ta^-$	3.00 ± 0.04	3.05 (0)	2.92 (0.41)	2.71 (0.47)	2.95 (0.46)

157 [a] Saddle points (no local minima were obtained with these symmetries).

158

159 To make our conclusion further convincing, we simulated photoelectron spectra of
160 $M@Ag_{12}^-$ with I_h, D_{5h}, O_h, and D_{3h} symmetries, where we utilized generalized Koopmans'
161 theorem[25] to evaluate the electron binding energies for photodetachment signals from h_g, $e''_1 + a'_1$
162 $+ e'_2$, $e_g + t_{2g}$, and $e'' + e' + a'_1$ orbitals. The evaluation yielded stick spectra corresponding to
163 photodetachment energies from each orbital with their relative intensities proportional to the
164 number of electrons occupying the orbital, as shown in Fig. 3. The stick spectra thus obtained were
165 broadened with a Lorentzian function with a full width at half maximum (FWHM) of 0.25, 0.28,
166 and 0.30 eV for $M@Ag_{12}^-$ (M = V, Nb, and Ta), respectively, which were obtained from the least-
167 squares fitting analysis mentioned in Fig. 3, to account for the spectral broadening in the
168 experiment; the spectral shape is determined by the instrumental function (see Fig. S1), the
169 Franck–Condon factor in the photodetachment process, and the spin–orbit coupling in the neutral
170 states. The photoelectron spectra thus simulated show that O_h and D_{5h} isomers both exhibit doublet

171 peaks. The ones simulated for D_{3h} structure are found to be asymmetric owing to the
172 photodetachment signal from the a'_1 orbital. Although further broadening makes their spectral
173 profiles symmetric, such spectra are too broad to reproduce the observed profiles. Thus, it is only
174 the I_h structure that can fully account for the experimental results. Electron binding energies
175 obtained by the other combinations of functionals and basis sets are summarized in Table S2 in
176 Supporting Information. The results are all consistent with the present one obtained by BP86/SDD
177 in terms of the splitting patterns of the 1D orbitals.

178 In the present study, we have succeeded in isomer-free production of $M@Ag_{12}^-$ (M = V,
179 Nb, and Ta) with I_h symmetry, which is contrasted to the cases of gold cages, $M@Au_{12}^-$ (M = V,
180 Nb, and Ta) investigated by Zhai et al.[14] The photodetachment spectra observed for the M-doped
181 gold cluster anions showed a main band at around 3.8 eV corresponding to the single band
182 observed for $M@Ag_{12}^-$ (M = V, Nb, and Ta) in the present study. While this main band is
183 assignable to icosahedral structures of $M@Au_{12}^-$, additional bands and broad backgrounds
184 superimposed on the main band were noticeable in each spectrum for $M@Au_{12}^-$ (M = V, Nb, and
185 Ta). The authors speculated that the spectra would have been contaminated with photodetachment
186 signals from anionic species with close mass-to-charge ratio, such as $Au_xM_yO_z^-$ and $Au_xM_y^-$, and
187 close-lying structural isomers with D_{5h} and O_h symmetries. The co-existence of the D_{5h} and O_h
188 isomers was indeed suggested by their DFT investigations, where these structural isomers were
189 found to be metastable.

190 Summarizing this work, we have obtained photoelectron spectra of the group 5 metal-
191 doped silver dodecamer anions, $Ag_{12}M^-$ (M = V, Nb, and Ta). Each spectrum commonly exhibits
192 only a single and nearly symmetric band, providing unambiguous experimental evidence that the
193 present $Ag_{12}M^-$ clusters have highly symmetric I_h geometries. Our DFT calculations revealed that

194 the I_h forms were indeed the most stable for all the clusters and that the possible highly-symmetric
195 structures with D_{5h}, O_h, and D_{3h} point groups were not found even in metastable states. The
196 photodetachment spectra simulated for icosahedral $M@Ag_{12}^-$ (M = V, Nb, and Ta) were in
197 excellent agreement with the experimental ones, fully supporting the above discovery.

198 $M@Ag_{12}^-$ (M = V, Nb, and Ta) discovered in the present work will offer an excellent
199 opportunity to study photoelectron angular distributions (PADs) from the 1S, 1P, and 1D electronic
200 shells that are the most *ideal* orbitals in the spherical jellium model. As shown in Figs. 1(d) – (f),
201 their PADs all exhibit a weak positive anisotropy to the laser polarization direction with the
202 photoelectron anisotropy parameters, β, of 0.54, 0.38, and 0.33 for M = V, Nb, and Ta, respectively.
203 Investigating how the β value varies as a function of the photoelectron kinetic energy, as has been
204 successfully demonstrated for Na_n^- by Bartels et al,[26] will enable us to characterize the fully
205 degenerate 1D electronic shell from the angular-momentum point of view. It is also interesting to
206 measure PADs from ligand-protected icosahedral cores of gold and silver clusters, whose
207 photodetachment spectra have been measured recently.[27] The study will address how ligands affect
208 PADs from discrete energy levels formed in gold and silver superatomic cores.

209

210

211 EXPERIMENTAL METHODS

212 The experiments were conducted using a photoelectron imaging apparatus for metal cluster
213 anions that we have built recently,[13] which allows for efficient measurements of photoelectron
214 images under space-charge free conditions. While a continuous-wave (CW) laser diode at 404 nm
215 (3.07 eV) was employed as a photodetachment light source in the original setup, we used fs UV
216 pulses at 310 nm (4.00 eV) in the present study, which were generated from an optical parametric

217 amplifier (ORPHEUS, Light Conversion) pumped by a Yb:KGW (ytterbium-doped potassium
218 gadolinium tungstate) regenerative amplifier (PHAROS PH2-10W, Light Conversion) that
219 delivers 1030 nm, ~210 fs, and 100 μJ pulses at a repetition rate of 100 kHz. The procedures for
220 acquiring photoelectron images of $M@Ag_{12}^-$ (M = V, Nb, and Ta) are given below.

221 A continuous beam of mass-selected $M@Ag_{12}^-$ (M = V, Nb, and Ta) cluster anions was
222 produced using a magnetron-sputtering cluster ion source, which was cooled with liquid nitrogen
223 at ~120 K, followed by a quadrupole mass filter.[28] The continuous cluster-anion beam was
224 transformed into ion bunches with a potential switch driven by a high voltage (+600 V) pulser
225 synchronized with the 100-kHz Yb:KGW regenerative amplifier. The bunched anion beam was
226 sent to an assembly of electrodes for extracting photoelectrons, which formed relatively low
227 (10 V/cm) static electric fields[29] optimized for a velocity-map imaging (VMI) condition,[30] where
228 the anions in the 100-kHz bunched beam were irradiated by linearly-polarized 310-nm fs pulses
229 with the average power of ~50 mW. Photoelectrons ejected from the anionic clusters were
230 accelerated toward a dual microchannel plate (ϕ40 mm) coupled with a P43 phosphor screen, on
231 which the 2D projection of the 3D photoelectron distribution was captured using a complementary
232 metal-oxide semiconductor camera (CS2100M-USB, 1920 × 1080, Thorlabs). Since a part of the
233 bunched anion beam itself created low energy electrons as it impinges on the VMI electrodes, we
234 subtracted a photoelectron image taken without the laser beam (i.e., laser-off image) from the laser-
235 on image to remove such backgrounds originated from the anion beam. The polar-onion-peeling
236 (POP) method[31] was used to reconstruct the original 3D distribution of the photoelectrons from
237 the subtracted image. As described in ref.[31], photodetachment spectra and laboratory-frame
238 photoelectron-angular distributions (PADs) were obtained through the reconstruction procedure.

Photoelectron kinetic energies (PKEs) were calibrated using the vertical detachment energy of Ag_3^- (2.43 eV),[32] which was done just after taking the data for $M@Ag_{12}^-$ by maintaining the temperature, *T*, of the magnetron sputtering source at ~120 K to produce also Ag_3^-. To evaluate the energy resolution and instrumental response of our VMI setup at PKEs comparable to those obtained for photoelectrons from $M@Ag_{12}^-$ (M = V, Nb, and Ta) with the 310-nm pulses, we measured a photoelectron image of Ag^- with a detachment laser tuned at 510 nm (2.43 eV), which was measured at $T \sim 300$ K; the abundance of Ag^- was not sufficient at $T \sim 120$ K. Fig. S1 in Supporting Information presents a photoelectron spectrum for Ag^- obtained from the photoelectron image. The energy resolution is evaluated to be 0.06 eV (~5%) at PKE = 1.13 eV.

AUTHOR INFORMATION

Corresponding Authors:

Takuya Horio − Department of Chemistry, Faculty of Science, Kyushu University, 744 Motooka, Nishi-ku, Fukuoka 819-0395, Japan; orcid.org/0000-0002-5769-6155;

Email: horio@chem.kyushu-univ.jp

Akira Terasaki − Department of Chemistry, Faculty of Science, Kyushu University, 744 Motooka, Nishi-ku, Fukuoka 819-0395, Japan; orcid.org/0000-0001-8293-0698;

Email: terasaki@chem.kyushu-univ.jp

Authors:

Yuta Suzuki − Department of Chemistry, Faculty of Science, Kyushu University, 744 Motooka, Nishi-ku, Fukuoka 819-0395, Japan

Kazuaki Matsumoto − Department of Chemistry, Faculty of Science, Kyushu University, 744 Motooka, Nishi-ku, Fukuoka 819-0395, Japan.

Rin Nomi − Department of Chemistry, Faculty of Science, Kyushu University, 744 Motooka, Nishi-ku, Fukuoka 819-0395, Japan

Masashi Arakawa − Department of Chemistry, Faculty of Science, Kyushu University, 744 Motooka, Nishi-ku, Fukuoka 819-0395, Japan; orcid.org/0000-0002-5954-8893

Notes

The authors declare no competing financial interests.

ASSOCIATED CONTENT

Supporting Information: The photodetachment spectrum of Ag^- obtained with incident photons at 2.43 eV and the results of the additional calculations of VDEs and electron binding energies for $Ag_{12}M^-$ (M = V, Nb, and Ta).

ACKNOWLEDGMENTS

This work was supported by Grants-in-Aid for Scientific Research (A) (JP18H03901 and 22H00317), Scientific Research (B) (JP22H02036), and Challenging Research (Exploratory) (JP20K21177 and JP22K19009) from the Japan Society for Promotion of Science (JSPS), the Asashi Glass Foundation, and Iketani Science and Technology Foundation. Experimental assistance by Tasuku Nishizato and Haruki Hashimoto is greatly acknowledged. The

computational work was carried out by the computer facilities at Research Institute for Information Technology, Kyushu University.

REFERENCES

(1) Kumar, V. Icosahedral Symmetry in Clusters. *Prog. Cryst. Growth. Charact. Mater.* **1997**, *34* (1–4), 95–131.

(2) Harris, I. A.; Kidwell, R. S.; Northby, J. A. Structure of Charged Argon Clusters Formed in a Free Jet Expansion. *Phys. Rev. Lett.* **1984**, *53* (25), 2390–2393.

(3) Echt, O.; Sattler, K.; Recknagel, E. Magic Numbers for Sphere Packings: Experimental Verification in Free Xenon Clusters. *Phys. Rev. Lett.* **1981**, *47* (16), 1121–1124.

(4) Mackay, A. L. A Dense Non-Crystallographic Packing of Equal Spheres. *Acta Crystallogr.* **1962**, *15* (9), 916–918.

(5) Castleman, A. W.; Khanna, S. N. Clusters, Superatoms, and Building Blocks of New Materials. *J. Phys. Chem. C* **2009**, *113* (7), 2664–2675.

(6) Jena, P.; Sun, Q. Super Atomic Clusters: Design Rules and Potential for Building Blocks of Materials. *Chem. Rev.* **2018**, *118* (11), 5755–5870.

(7) Takano, S.; Tsukuda, T. Chemically Modified Gold/Silver Superatoms as Artificial Elements at Nanoscale: Design Principles and Synthesis Challenges. *J. Am. Chem. Soc.* **2021**, *143* (4), 1683–1698.

(8) Zhao, J.; Du, Q.; Zhou, S.; Kumar, V. Endohedrally Doped Cage Clusters. *Chem. Rev.* **2020**, *120* (17), 9021–9163.

(9) Pyykkö, P.; Runeberg, N. Icosahedral WAu_{12}: A Predicted Closed-Shell Species, Stabilized by Aurophilic Attraction and Relativity and in Accord with the 18-Electron Rule. *Angew. Chem. Int. Ed.* **2002**, *41* (12), 2174.

(10) de Heer, W. A. The Physics of Simple Metal Clusters: Experimental Aspects and Simple Models. *Rev. Mod. Phys.* **1993**, *65* (3), 611–676.

(11) Li, X.; Kiran, B.; Li, J.; Zhai, H.-J.; Wang, L.-S. Experimental Observation and Confirmation of Icosahedral $W@Au_{12}$ and $Mo@Au_{12}$ Molecules. *Angew. Chem. Int. Ed.* **2002**, *41* (24), 4786–4789.

(12) Minamikawa, K.; Sarugaku, S.; Arakawa, M.; Terasaki, A. Electron Counting in Cationic and Anionic Silver Clusters Doped with a 3d Transition-Metal Atom: Endo- *vs.* Exohedral Geometry. *Phys. Chem. Chem. Phys.* **2022**, *24* (3), 1447–1455.

(13) Horio, T.; Minamikawa, K.; Nishizato, T.; Hashimoto, H.; Matsumoto, K.; Arakawa, M.; Terasaki, A. Photoelectron Imaging of Size-Selected Metal Cluster Anions in a Quasi-Continuous Mode. *Rev. Sci. Instrum.* **2022**, *93* (8), 083302.

(14) Zhai, H.-J.; Li, J.; Wang, L.-S. Icosahedral Gold Cage Clusters: M@Au_{12}^{-} (M=V, Nb, and Ta). *J. Chem. Phys.* **2004**, *121* (17), 8369–8374.

(15) Häkkinen, H.; Yoon, B.; Landman, U.; Li, X.; Zhai, H.-J.; Wang, L.-S. On the Electronic and Atomic Structures of Small Au_N^{-} (N = 4−14) Clusters: A Photoelectron Spectroscopy and Density-Functional Study. *J. Phys. Chem. A* **2003**, *107* (32), 6168–6175.

(16) Handschuh, H.; Cha, C.; Bechthold, P. S.; Ganteför, G.; Eberhardt, W. Electronic Shells or Molecular Orbitals: Photoelectron Spectra of Ag_n^{-} Clusters. *J. Chem. Phys.* **1995**, *102* (16), 6406–6422.

(17) Medel, V. M.; Reber, A. C.; Chauhan, V.; Sen, P.; Köster, A. M.; Calaminici, P.; Khanna, S. N. Nature of Valence Transition and Spin Moment in Ag_nV^{+} Clusters. *J. Am. Chem. Soc.* **2014**, *136* (23), 8229–8236.

(18) Frisch, M. J.; Trucks, G. W.; Schlegel, H. B.; Scuseria, G. E.; Robb, M. A.; Cheeseman, J. R.; Scalmani, G.; Barone, V.; Petersson, G. A.; Nakatsuji, H.; Li, X.; Caricato, M.; Marenich, A. V.; Bloino, J.; Janesko, B. G.; Gomperts, R.; Mennucci, B.; Hratchian, H. P.; Ortiz, J. V.; Izmaylov, A. F.; Sonnenberg, J. L.; Williams-Young, D.; Ding, F.; Lipparini, F.; Egidi, F.; Goings, J.; Peng, B.; Petrone, A.; Henderson, T.; Ranasinghe, D.; Zakrzewski, V. G.; Gao, J.; Rega, N.; Zheng, G.; Liang, W.; Hada, M.; Ehara, M.; Toyota, K.; Fukuda, R.; Hasegawa, J.; Ishida, M.; Nakajima, T.; Honda, Y.; Kitao, O.; Nakai, H.; Vreven, T.; Throssell, K.; Montgomery, J. A. Jr.; Peralta, J. E.; Ogliaro, F.; Bearpark, M. J.; Heyd, J. J.; Brothers, E. N.; Kudin, K. N.; Staroverov, V. N.; Keith, T. A.; Kobayashi, R.; Normand, J.; Raghavachari, K.; Rendell, A. P.; Burant, J. C.; Iyengar, S. S.; Tomasi, J.; Cossi, M.; Millam, J. M.; Klene, M.; Adamo, C.; Cammi, R.; Ochterski, J. W.; Martin, R. L.; Morokuma, K.; Farkas, O.; Foresman, J. B.; Fox, D. J.; Gaussian, Inc. , W. C. 2016. Gaussian 16, Revision C.01.

(19) Perdew, J. P. Density-Functional Approximation for the Correlation Energy of the Inhomogeneous Electron Gas. *Phys. Rev. B* **1986**, *33* (12), 8822–8824.

(20) Becke, A. D. Density-Functional Exchange-Energy Approximation with Correct Asymptotic Behavior. *Phys. Rev. A* **1988**, *38* (6), 3098–3100.

(21) Perdew, J. P.; Burke, K.; Ernzerhof, M. Generalized Gradient Approximation Made Simple. *Phys. Rev. Lett.* **1996**, *77* (18), 3865–3868.

(22) Dolg, M.; Wedig, U.; Stoll, H.; Preuss, H. Energy-adjusted *ab initio* Pseudopotentials for the First Row Transition Elements. *J. Chem. Phys.* **1987**, *86* (2), 866–872.

(23) Andrae, D.; Häußermann, U.; Dolg, M.; Stoll, H.; Preuß, H. Energy-adjusted *ab initio* Pseudopotentials for the Second and Third Row Transition Elements. *Theor. Chim. Acta* **1990**, *77* (2), 123–141.

(24) Hay, P. J.; Wadt, W. R. *Ab Initio* Effective Core Potentials for Molecular Calculations. Potentials for K to Au Including the Outermost Core Orbitals. *J. Chem. Phys.* **1985**, *82* (1), 299–310.

(25) Tozer, D. J.; Handy, N. C. Improving Virtual Kohn–Sham Orbitals and Eigenvalues: Application to Excitation Energies and Static Polarizabilities. *J. Chem. Phys.* **1998**, *109* (23), 10180–10189.

(26) Bartels, C.; Hock, C.; Huwer, J.; Kuhnen, R.; Schwöbel, J.; von Issendorff, B. Probing the Angular Momentum Character of the Valence Orbitals of Free Sodium Nanoclusters. *Science* **2009**, *323* (5919), 1323–1327.

(27) Ito, S.; Tasaka, Y.; Nakamura, K.; Fujiwara, Y.; Hirata, K.; Koyasu, K.; Tsukuda, T. Electron Affinities of Ligated Icosahedral M_{13} Superatoms Revisited by Gas-Phase Anion Photoelectron Spectroscopy. *J. Phys. Chem. Lett.* **2022**, *13* (22), 5049–5055.

(28) Sarugaku, S.; Arakawa, M.; Kawano, T.; Terasaki, A. Electronic and Geometric Effects on Chemical Reactivity of 3d-Transition-Metal-Doped Silver Cluster Cations toward Oxygen Molecules. *J. Phys. Chem. C* **2019**, *123* (42), 25890–25897.

(29) Horke, D. A.; Roberts, G. M.; Lecointre, J.; Verlet, J. R. R. Velocity-Map Imaging at Low Extraction Fields. *Rev. Sci. Instrum.* **2012**, *83* (6), 063101.

(30) Eppink, A. T. J. B.; Parker, D. H. Velocity Map Imaging of Ions and Electrons Using Electrostatic Lenses: Application in Photoelectron and Photofragment Ion Imaging of Molecular Oxygen. *Rev. Sci. Instrum.* **1997**, *68* (9), 3477–3484.

(31) Roberts, G. M.; Nixon, J. L.; Lecointre, J.; Wrede, E.; Verlet, J. R. R. Toward Real-Time Charged-Particle Image Reconstruction Using Polar Onion-Peeling. *Rev. Sci. Instrum.* **2009**, *80* (5), 053104.

(32) Ho, J.; Ervin, K. M.; Lineberger, W. C. Photoelectron Spectroscopy of Metal Cluster Anions: Cu_n^-, Ag_n^-, and Au_n^-. *J. Chem. Phys.* **1990**, *93* (10), 6987–7002.